JGR Atmospheres

RESEARCH ARTICLE
10.1029/2019JD030796

A New Engineering Model of Lightning M Component That Reproduces Its Electric Field Waveforms at Both Close and Far Distances

Mohammad Azadifar[1], Marcos Rubinstein[1], Quanxin Li[2,3], Farhad Rachidi[3], and Vladimir Rakov[4,5]

[1]University of Applied Sciences of Western Switzerland, Yverdon-les-Bains, Switzerland, [2]School of Electrical Engineering and Automation, Wuhan University, Wuhan, China, [3]Electromagnetic Compatibility Laboratory, Swiss Federal Institute of Technology (EPFL), Lausanne, Switzerland, [4]Department of Electrical and Computer Engineering, University of Florida, Gainesville, FL, USA, [5]Moscow Institute of Electronics and Mathematics, National Research University Higher School of Economics, Moscow, Russia

Key Points:

- The new engineering M component model can reproduce the microsecond-scale electric field pulses thought to be due to the junction process
- The proposed model can be used to simulate both the microsecond- and millisecond-scale features of M component field signatures at close and far ranges
- The geometry of the in-cloud leader channel and the junction point height largely determine the presence of the microsecond-scale electric field pulses

Correspondence to:
M. Azadifar,
mohammad.azadifar@heig-vd.ch

Citation:
Azadifar, M., Rubinstein, M., Li, Q., Rachidi, F., & Rakov, V. (2019). A new engineering model of lightning M component that reproduces its electric field waveforms at both close and far distances. *Journal of Geophysical Research: Atmospheres*, *124*, 14,008–14,023. https://doi.org/10.1029/2019JD030796

Received 10 APR 2019
Accepted 20 NOV 2019
Accepted article online 26 NOV 2019
Published online 16 DEC 2019

Abstract We present a new engineering model for the M component mode of charge transfer to ground that can predict the observed electric field signatures associated with this process at various distances, including (a) the microsecond-scale pulse thought to be due to the junction of in-cloud leaders and the grounded, current-carrying channel and (b) the ensuing slow, millisecond-scale pulse due to the M component proper occurring below the junction point. We examine the features of 13 microsecond-scale, fast electric field pulses associated with M component processes in upward negative lightning initiated from the Säntis Tower and recorded 14.7 km from it. Eleven out of the 13 pulses were found to be unipolar with pulse widths in the range of 9.8 to 35 μs, and the other two were bipolar. To model the process that gives rise to microsecond-scale pulses, we hypothesize that the current pulses propagating away from the junction point along the main lightning channel (below the junction point) and along the feeding in-cloud leader channel (branch) carry the same amount of charge. We further assume that the pulse traversing the branch is similar to a subsequent return-stroke (RS) pulse. In the model, the RS-like process is represented by the MTLE model. The millisecond-scale field signature that follows the initial fast pulse in M components at close distances is simulated in our model using the guided-wave M component model. The proposed model successfully reproduces the vertical electric field waveforms associated with M-component processes in upward lightning flashes initiated from the Säntis Tower at 14.7-km distance from the lightning channel, in which both the fast, microsecond-scale and the following slower, millisecond-scale pulses were observed. The model also reasonably reproduces the known features of electric field signatures at close distances (up to 5 km), where the amplitude of the millisecond-scale hook-like pulse is much larger than that of the microsecond-scale pulse, and at far distances (of the order of 100 km), where the microsecond-scale pulses are dominant.

1. Introduction

Three basic modes of charge transfer to ground associated with cloud-to-ground lightning discharges have been identified to date: (1) The leader/return stroke (RS) mode of charge transfer, (2) the continuing current (CC) mode of charge transfer, and (3) the M component mode of charge transfer (Rakov et al., 2001). These three modes have been observed both in downward and in upward lightning flashes (Miki et al., 2005).

The M-component mode of charge transfer takes its name from the term "M components." M components were first described as intensifications in the luminosity of lightning channels in downward lightning (Malan & Collens, 1937). Based on channel-base current measurements in triggered lightning experiments, Fisher and co-workers (Fisher et al., 1993) reported that M components are linked to current pulses during the slow CC that follows some RSs, having an amplitude of tens to hundreds of amperes and lasting from less than 10 to hundreds of milliseconds. M components also occur during the initial stage in upward lightning and rocket-triggered lightning.

When measured at the channel base, the current pulses associated with the M component mode of charge transfer exhibit a more or less symmetrical waveshape (Fisher et al., 1993; He et al., 2018; Paul & Heidler, 2018; Thottappillil et al., 1995; Visacro et al., 2013) and they are responsible for the above mentioned transient enhancement in the channel luminosity (Campos et al., 2007; Flache et al., 2008; Jordan

et al., 1995; Malan & Schonland, 1947; Qie et al., 2011; Stolzenburg et al., 2015; Winn et al., 2012; Zhou et al., 2014).

The characteristics of M component current pulses at the channel base are found to be different from those of RS pulses (Thottappillil et al., 1995). The reported geometric mean of the 10% to 90% risetime and of the current peak of M components were 422 μs and 117 A, respectively. They also found that the first M component occurs within 4 ms after the RS. A similar conclusion was arrived at by Campos et al. (2007) who used high-speed video camera observations. A thorough statistical analysis of the channel-base current features of M components, including total charge, duration, and amplitude of the pulses in comparison with RS pulses, was also given by Zhang et al. (2016).

Using streak-camera records of two M components during a downward lightning flash, Jordan et al. (1995) found, for one of their recorded events, that the amplitude and waveshape of the luminosity did not vary with height. For another event, they found a slight decrease in the amplitude of light with increasing height.

Using optical measurements along with channel-base current measurements, Flache et al. (2008) reported that current pulses with risetimes longer than 8 μs corresponded to the M component mode of charge transfer to ground and those with risetimes shorter than 8 μs were associated with the leader-RS mode.

The electric field from M component processes is characterized by a millisecond-scale, hook-like shape pulse at distances of up to a few kilometers (Malan & Schonland, 1947). Rakov et al. (1992) analyzed M component electric field waveforms at distances of 2.5 to 27 km. They observed one or several microsecond-scale fast pulses in the initial part of 70% of the slow hook-like shape pulses. At longer distances of 45 to 128 km, the fast pulse is observed to become dominant and the slow, hook-like shape waveform is generally not discernible (Tran et al., 2013; Wang et al., 2017).

Zhou et al. (2015) used the term "mixed mode" of charge transfer to describe the transfer of charge associated with faster pulses (compared to M component-type pulses) superimposed on the initial continuous current (ICC) in upward negative flashes. The name mixed mode was given to this mode of charge transfer by Zhou et al. (2015) because of their observation of two distinct channels sharing only their lower part, one of the channels supporting the CC mode of charge transfer and the other the leader/RS mode of charge transfer. They used the time difference between the peak of the electric field and the onset of the current as a criterion to distinguish between the different modes of charge transfer.

The pulses associated with the mixed mode of charge transfer mentioned above exhibit faster risetimes than M component-type pulses and are asymmetrical in shape. They are associated with the junction of a leader to an already luminous ICC channel at junction point heights that are low, typically lower than 1 km or so, compared to the junction point heights observed for "classical" M component-type processes (Zhou et al., 2015).

Using an interferometer along with field measurements in downward lightning flashes, Shao et al. (1995) found that an M component-like process could occur upon the connection of a recoil leader to a CC-carrying channel. They also observed that within a few milliseconds after the arrival of the RS to the source region in the cloud, fast positive streamers propagate away from the source region and they are followed by fast negative streamers that retrace the positive streamer channel. These recoil streamers, with estimated speeds of 10^6 to 10^7 m/s, introduce negative charge into the cloud-to-ground channel, thus leading to the M component mode of charge transfer. They observed that microsecond-scale electric field pulses occur upon the connection of the recoil leader to the current-carrying channel.

Using interferometer observations along with channel-base currents and close electric field measurements (92 to 357 m), Yoshida et al. (2012) investigated the mechanism of charge transfer during the initial stage of rocket-and-wire-triggered lightning. They inferred that M component-like pulses during the initial stage of the flash can be initiated either by recoil leaders in decayed branches (short-duration leaders) or by separate in-cloud leaders (long-duration leaders).

Mazur and Ruhnke (2011) proposed an electrostatic model for the formation of what they referred to an "M-event" process. In their model, after the attachment of a newly formed branch or a reactivated branch to the main channel of an upward negative lightning, the branch behaves in a manner similar to that of other UPL (upward positive leader) branches (see their Figure 22). The authors also proposed a similar model for

dart leader/RS processes, in which upon arrival of the dart leader to the ground, an impulsive RS process occurs (see their Figure 21). Mazur and Ruhnke (2011) did not consider the transient process in the main channel, which is the M component proper.

Rakov et al. (1995), considering simultaneously measured channel-base currents and close electric fields (30 m) for the M component process, proposed a guided-wave (two-wave) mechanism, in which a downward moving current wave would be followed by an upward moving wave of the same polarity. The model proposed by Rakov et al. (2001, 1995) was implemented in some studies to reproduce the millisecond-scale electromagnetic field signature of the M component process (He et al., 2018; Jiang et al., 2013; Zhang et al., 2011). Optical evidence in support of the guided-wave mechanism of M components is reported by Jiang et al. (2014). However, the above models cannot reproduce the fast, microsecond-scale pulses observed at larger distances from the lightning channel, up to about 130 km (Rakov et al., 1992, 1996; Tran et al., 2013; Wang et al., 2017).

Warner et al. (2016) recorded high-speed video images of a bidirectional leader whose negative end connected to a luminous upward positive leader channel and, upon the connection, observed a fast pulse in the associated electric field recorded at 18 km.

Tran and Rakov (2019) recently developed an advanced (distributed-circuit) model of M components that takes into account transient processes both in the grounded channel and in the in-cloud channel making connection to it but tested their model only against the field measured at close distances.

In this paper, using observed features of M component luminosity and recorded electric fields presented in the literature, we propose a new engineering model that can predict both the millisecond- and the microsecond-scale electric field pulses of the M component process at various distances. Our model describes the transient processes both in the main channel (M component proper) and in the newly connected or reenergized branch (the excitation source), each contributing to the distant electromagnetic signatures of M components. The proposed model can be used to infer the height of the junction process. However, more validation measurements are required in this regard using either optical observations or VHF imaging techniques such as Lightning Mapping Array (LMA) and interferometry.

The M component events used in this paper for the validation process are associated with M component pulses in upward lightning flashes. The similarity between M components in the CC of downward lightning flashes and M component pulses in the ICC in upward lightning was established by He, Azadifar, Li, et al. (2018). As a result, the same mathematical modeling is applicable to the M components associated with downward flashes.

This paper is organized as follows. Section 2 briefly reviews the current and electric field measurement stations installed at and near the Säntis Tower; data acquired at these stations were used to test the validity of the proposed model. In section 3, we discuss the features of the fast microsecond-scale pulses. A possible scenario and mathematical modeling of the M component process are presented in sections 4 and 5, respectively. Simulations and results are given in section 6. Finally, summary is given in section 7.

2. Current and Field Measurement Stations

The Säntis Tower is 124 m tall, and it sits on top of the 2,502-m tall Mount Säntis located at 47°14′57″N and 9°20′32″E in the Appenzell region in northeastern Switzerland. The Säntis Tower was instrumented in May 2010 for the direct measurement of lightning currents (see Romero et al., 2012, for detailed information on the instrumentation and Azadifar et al., 2014, for upgrades made in 2013–2014).

A wideband electric field measurement station was deployed on 23 July 2014, and it was operational until 28 October 2014 to record electric fields associated with lightning striking the Säntis Tower. The electric and magnetic field sensors were installed on the roof of a 25-m tall building belonging to Huber+Suhner in Herisau, 14.7 km away from the tower.

The system included two Thales (former Thomson CSF) Mélopée sets for the measurement of the vertical electric field and the azimuthal magnetic field. The operating frequency bandwidth of the system was 2 kHz to 150 MHz, and the time constant of the system was about 160 μs. To compensate for the effect of

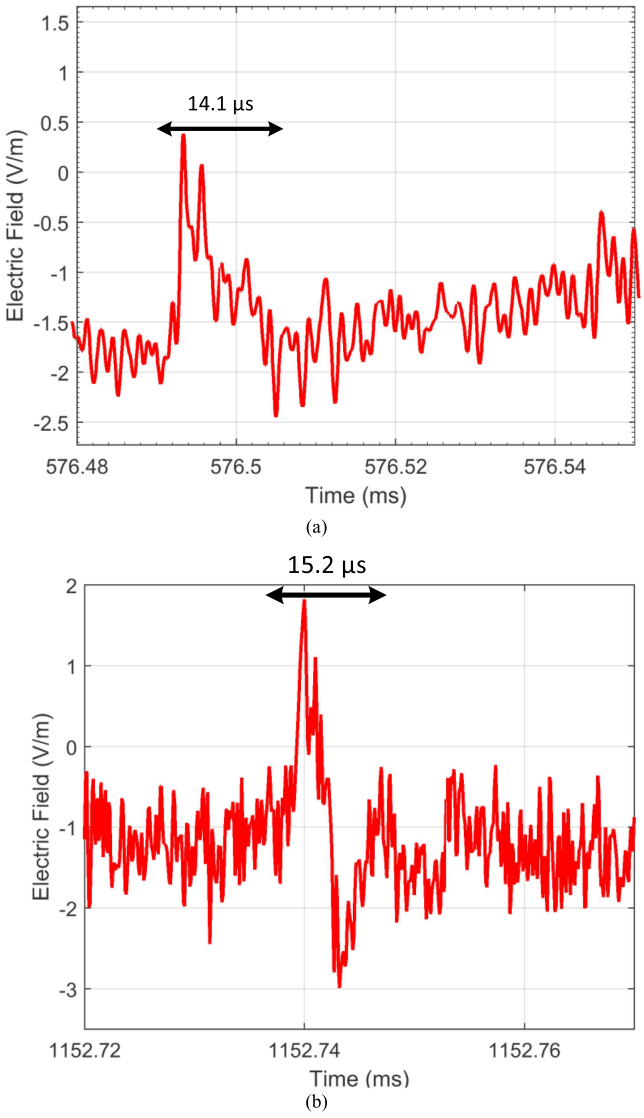

Figure 1. Fast connecting pulses observed about 15 km away from the lightning channel. (a) A unipolar pulse with initial positive excursion (the pulse width is about 14.1 μs). (b) A bipolar pulse with initial positive excursion (the overall pulse width is about 15.2 μs).

the relatively short time constant of the system, the methodology proposed by Rubinstein et al. (2012) was applied to the recorded electric field waveforms.

It should be noted that the channel-base current and electric field waveforms were synchronized using the pattern of interpulse intervals since GPS time stamps were not available for the events used in this paper.

3. Characteristics of the Microsecond-Scale Fast Pulses

We now briefly review the observed features of the fast electric field pulses associated with the M components reported in the literature, and we present the characteristics of similar field pulses measured at the Säntis Tower facility (in Herisau, 14.7 km away from the tower).

Fast electric field pulses that mark the start of the M component process were named microsecond-scale pulses by Rakov et al. (1992). They found that microsecond-scale pulses associated with M components were often irregular. They observed one pulse or multiple pulses of bipolar or unipolar waveshapes within the initial portion of the hook with either the same or opposite polarity with respect to the hook-shaped pulse. Shao et al. (1995) observed that fast pulses occur upon the connection of fast negative recoil leaders with the previously formed main positive leader channel inside the cloud. The first microsecond-scale electric field signature of M components and the corresponding current waveform were reported by Rakov et al. (2001). Based on measurements at 7 and 18-km distances, Warner et al. (2016) observed similar fast electric field pulses upon the connection of the negative end of bidirectional leaders with existing, still developing upward positive leaders.

Tran et al. (2013) detected microsecond-scale electric field pulses only in 1/3 to 1/2 of the M component pulses at 45 km from the rocket-triggered lightning flashes. They reported that the time difference between these fast pulses and the starting point of the channel-base current in their dataset was in the range of 1 to 120 μs for fields recorded at 45 km.

Here, we present characteristics of individual microsecond-scale fast pulses in our electric field records 14.7 km away from the lightning channel. Note that the atmospheric electricity sign convention is used to represent electric field waveforms throughout this paper.

We observed that the microsecond-scale fast pulses (which we will call fast connecting pulses) could be bipolar or unipolar. Both the initial polarity of the bipolar pulses and the polarity of the unipolar pulses were the same as that of the slow M component pulse field, which was in turn the same as that of RSs in negative cloud-to-ground lightning. Figure 1 shows two examples of fast connecting pulses with unipolar and bipolar pulse shapes, with pulse widths of about 14.1 and 15.2 μs, respectively. Table 1 presents characteristics of 13 fast connecting pulses, including pulse shape, initial polarity, and pulse width. These 13 pulses were selected since they are large enough for their waveshape to be distinguishable from the background noise. The majority of the pulses are unipolar, and the pulse widths range from 9.8 to 35 μs. It should be noted that due to the background noise, pulse width values are only rough estimates.

4. Proposed Scenario for M Component Process

In this section, we review the observations presented in various studies on the M component mode of charge transfer to ground and propose a possible scenario, which can predict the full electric field signature at various distances, including the fast, microsecond-scale field pulses.

Table 1
Characteristics of Fast Connecting Pulses

Count	Pulse shape	Initial polarity	Pulse width (μs)
1	unipolar	+	9.8
2	unipolar	+	10.4
3	unipolar	+	25.4
4	bipolar	+	20
5	unipolar	+	15.3
6	unipolar	+	14.1
7	unipolar	+	11.6
8	unipolar	+	13.1
9	unipolar	+	12.1
10	unipolar	+	15.5
11	unipolar	+	35
12	unipolar	+	16.2
13	bipolar	+	15.2

1- The electric field waveforms associated with M component processes are characterized by a millisecond-scale, hook-like shape pulse that is clearly visible at close distances and that can be reproduced by simulation using the guided-wave model proposed by Rakov et al. (2001, 1995). More recently, He, Azadifar, Rachidi, et al. (2018) used the guided-wave model to reproduce millisecond-scale electric field pulses at a distance of 15 km from the lightning channel.

2- Microsecond-scale electric field pulses have been observed to appear upon the connection of a negative leader to the already luminous main conducting lightning channel (Shao et al., 1995). Warner et al. (2016) observed microsecond-scale fast pulses upon the connection of a bidirectional leader to both upward and downward developing positive leaders. These field pulses have been observed at distances up to 126 km (Wang et al., 2017). This observation implies that a highly transient process occurs upon connection of a floating (in-cloud) channel to the main grounded channel.

3- High-speed video images of a bidirectional leader that attaches to a preexisting positively charged lightning channel were recorded by Montanyà et al. (2015) during an IC flash. They observed that upon the connection of the negative end of a bidirectional leader to the positively charged end of in-cloud channel, the luminosity of the main in-cloud channel increased on one side of the junction point only (see their Figure 3). Also, a bright luminosity front traveled from the connection point outward through the negative end of the bidirectional leader, past the initiation point, and out to the positive end of the bidirectional leader. Montanyà et al. (2015) described this luminosity as a RS-like process.

Based on the above mentioned observations and discussion, we propose a possible scenario which, as we will see, can reproduce the observed *E* field records, including both the fast connecting pulses and the following slow pulses, at 14.7 km from the channel, as well as the observed features of the fields at closer and at longer distances.

The fact that the current in the mixed-mode of charge transfer to ground is associated with low junction points and with channel-base current pulses with fast risetimes, similar to RSs, suggests that the current in the branch propagates into the main channel. If that is also the case for the higher junction points associated with M components, then it is possible that the slow M component current waveshapes observed at the base of the channel stem from the effects of propagation along the main channel to the ground. Tran and Rakov (2019), who modeled M components using a nonlinear distributed circuit model, reported significant differences in the current (and power) waveform frequency content near the ground level and aloft. The higher-frequency components present near the junction point were largely "filtered out" within a few kilometers of that point. In our model, we used an engineering approach to account for the transition from branch to main channel in which the link between the current in the branch and the current in the main channel is only based on the total charge contained in the respective pulses, while using for the main channel the guided-wave mechanism that has been tested in the literature (e.g., (He, Azadifar, Rachidi, et al., 2018). This approach simplifies the model, and, as we will see, it yields good agreement between the model-predicted and experimental results.

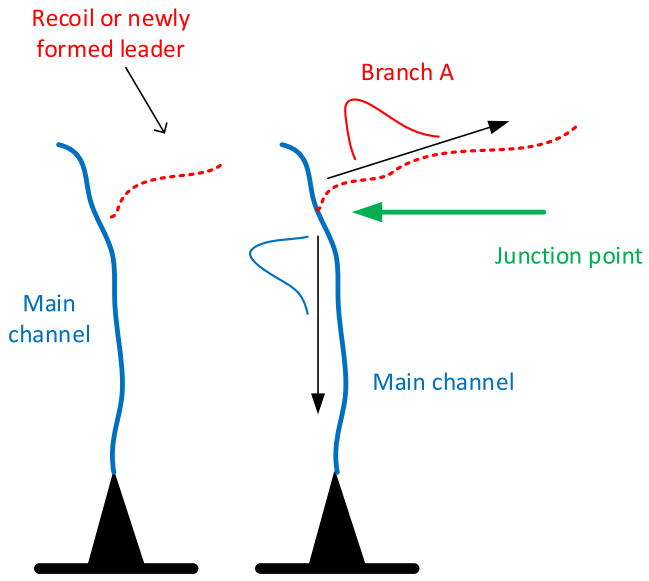

Figure 2. The proposed model. Left panel: Channel geometry prior to connection of approaching leader. Right panel: Channel geometry after connection of the leader to the main channel launching current waves along both the main channel and Branch A, away from the junction point.

Figure 2 illustrates schematically the main grounded channel, which facilitates the CC mode of charge transfer to ground (in blue). A negative in-cloud leader labeled "Branch A" (a recoil or newly formed leader), shown as a dashed red line, approaches the main channel.

- Upon connection of the main channel and Branch A, negative charges carried by the branch will be introduced into the main channel, which

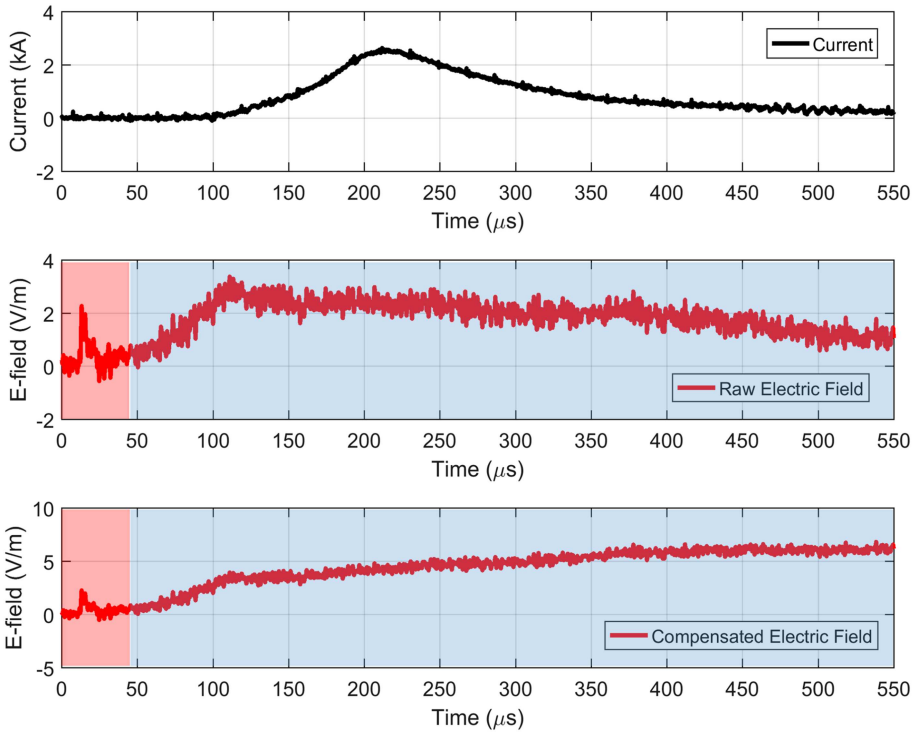

Figure 3. An example of simultaneous channel-base current and raw and compensated vertical E field waveforms. The waveforms are part of an upward negative flash initiated from the Säntis Tower, which occurred on 21 October 2014, at 20:42:50 (local time).

is assumed to be at nearly ground potential. A neutralization wave similar to a RS process travels away from the junction point along Branch A (see the pulse and arrow pointing away from the main channel in the right panel of Figure 2). Similar to the RS current pulse, this current pulse is expected to have a short risetime. This scenario is consistent with the optical observations by Montanyà et al. (2015), although their main channel was not grounded.

- The neutralization in Branch A drains positive charges from the main channel. As a result, a negative current wave moves downward in the main, current-carrying channel and undergoing attenuation and dispersion in its path, as expected for M component waves (Tran & Rakov, 2019). This downward wave gets reflected off the top of the tall object, and the reflection moves upward (guided-wave mechanism).

5. Mathematical Modeling

Figure 3 shows an example of an M component-like pulse including its measured channel-base current, measured electric field waveform at 14.7 km, and time-constant-compensated electric field waveform. This event occurred on 21 October 2014 at 20:42:50 (local time) in a negative upward lightning discharge initiated from the Säntis Tower. The part of the E field plot highlighted in red up to 50 μs shows the microsecond-scale electric field pulse, and the rest of the plot highlighted in blue shows the millisecond-scale pulse.

Figure 4 shows a schematic diagram of the proposed model. The adjustable parameters for the main channel, modeled as a straight and vertical line, and for the branch that influence the temporal and spatial distribution of the current are given in the diagram. We will use $i_1(z,t)$ and $i_0(r,t)$ to represent the current distribution along the main channel and Branch A, respectively. For the current in the branch, r is measured along the branch starting at the junction point. To calculate the fields from Branch A, the basic field equations for a straight and vertical channel were modified by way of geometrical translations and rotations. The details of these operations are not presented here.

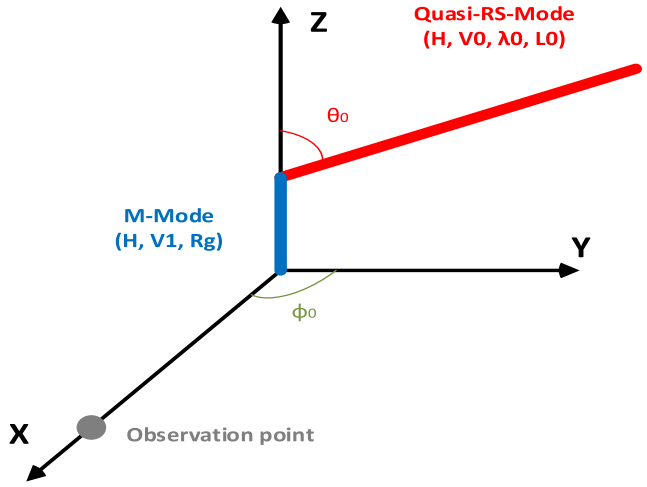

Figure 4. Schematic diagram of the proposed model with input parameters corresponding to the main channel and the branch. The adjustable parameters are (i) height of the main channel H, velocity of the M component wave v_1, and reflection coefficient at ground level R_g, for the main channel, and, (ii) return stroke velocity v_0, attenuation constant λ_0, length of the branch L_0, inclination angle (θ_0), and azimuth angle (φ_0), for the Branch A.

As discussed in sections 1 and 4, the M component model based on the guided-wave mechanism proposed by Rakov et al. (2001, 1995) can reproduce the slow, millisecond-scale electric field waveform from an M component process. We employed that model in this paper to calculate the fields due to the current waves in the main channel. Note that the current above the junction point is assumed to be zero. The distribution of the current along the main channel is given by equation (1)

$$\begin{aligned} i_1(z',t) &= i_1(H, t-(H-z')/v_1) && t<H/v_1 \\ i_1(z',t) &= i_1(H, t-(H-z')/v_1) + R_g \times i_1(H, t-(H+z')/v_1) && t\geq H/v_1 \end{aligned} \quad (1)$$

in which

- H is the height of the junction point,
- v_1 is the velocity of the incident and the reflected current waves,
- R_g is the current reflection coefficient at ground level, and
- $i_1(H,t)$ is the current injected at the junction point. This current can be obtained from the current measured at the channel base ($i_1(0,t)$) by setting $z' \rightarrow 0$ and $t \rightarrow t+H/v_1$.

As stated in section 4, we consider a RS-like process (based on the MTLE model) in Branch A, given by equation (2). The current as a function of time and of the position along Branch A, which according to the MTLE model (Nucci et al., 1988; Rachidi & Nucci, 1990), is given by

$$i_0(r,t) = \exp(-r/\lambda_0) \times i_c(t-r/v_0) u(t-r/v_0) \quad (2)$$

in which $i_c(t)$ is the current at the junction point propagating along Branch A, λ_0 is the attenuation constant, and v_0 is the propagation velocity. The current in the main channel is only observable after it has propagated down to the tower, since the current measuring instrumentation is installed on the tower. The exact mechanism of charge neutralization and redistribution upon the attachment of Branch A to the main channel is not known. In addition, the electrical properties of both the main channel and Branch A are possibly time varying and nonlinear (see Tran & Rakov, 2019). As a result, $i_c(t)$ cannot be retrieved from the measured channel-base current due to the unknown attachment mechanism, dispersion, and attenuation along the main channel.

Absent any experimental way to determine the current in the branch and based on the description by Montanyà et al. (2015) of the luminosity wave in a newly connected branch as a RS-like process, we used the typical subsequent RS current waveform ($i_{typ}(t)$) proposed by Rachidi et al. (2001) to specify the shape of $i_c(t)$. These typical waveforms are represented by the sum of two Heidler functions whose parameters are given in Table 2. The only constraint that we have imposed is conservation of charge at the junction point during the entire process. Imposing this condition, $i_c(t)$ can be found using equation (3):

$$\begin{aligned} i_c(t) &= i_{typ}(t) \times q \\ q &= \frac{\int_0^\infty i_1(H,t')dt'}{\int_0^\infty i_{typ}(t')dt'} \end{aligned} \quad (3)$$

Table 2
Parameters of Heidler functions used to represent typical subsequent return stroke

Heidler function parameters (1)		Heidler function parameters (2)	
I_1 (kA)	10.7	I_2 (kA)	6.5
τ_{11} (μs)	0.25	τ_{21} (μs)	2.1
τ_{12} (μs)	2.5	τ_{22} (μs)	230
N_1	2	N_2	2

6. Simulations and Results

In this section, we examine the ability of the proposed model to reproduce the electric field signatures of the M component process at various distances. We will first compare the electric field waveforms predicted

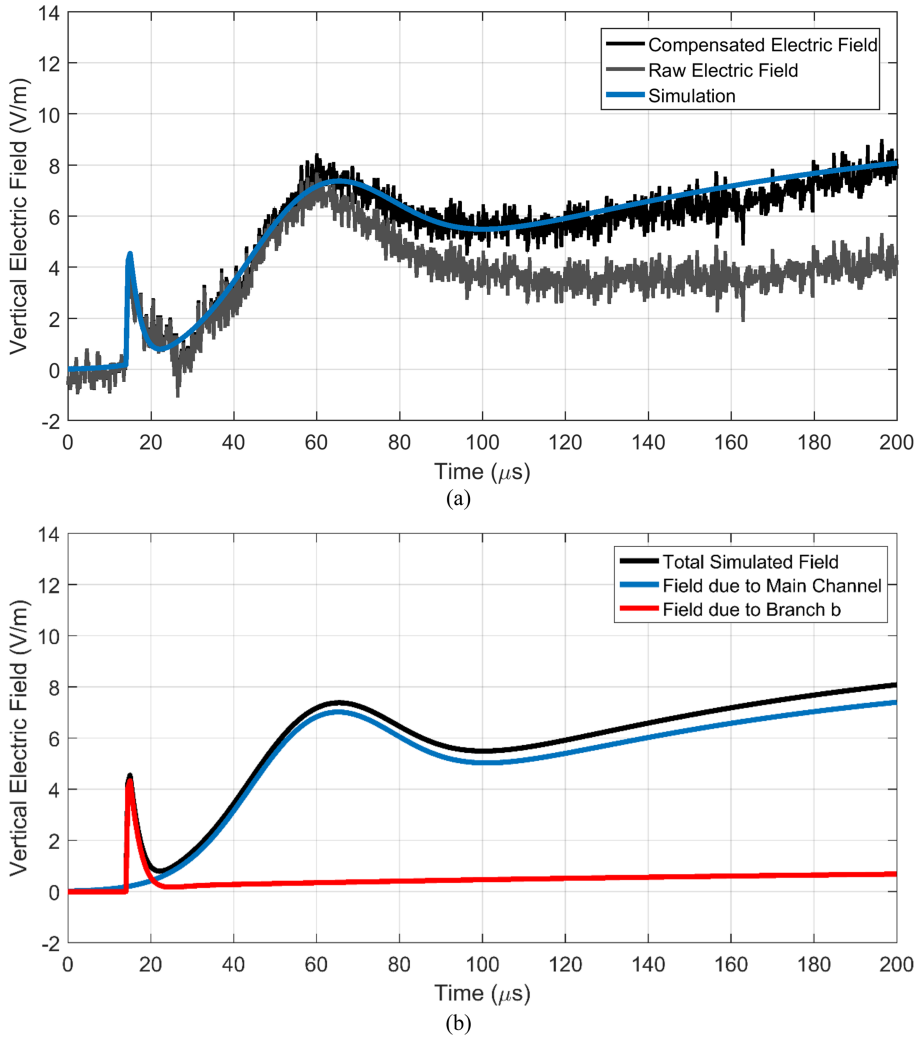

Figure 5. Vertical electric field computed using the model proposed in this paper. The lightning flash occurred on 21 October 2014, at 20:42:50. (a) Simulated vertical electric field versus measured field. (b) Contribution of main channel and of Branch A to the total electric field.

by the model to the measured electric fields at 14.7 km, using the measured channel-base current waveforms. We will then present a discussion of the effects of the variation of the model parameters, and we will show the ability of the model to predict the observed electric field waveforms of M components at other distances. Finally, we will propose a definition of close and middle-and-far range distances based on the present model.

6.1. Ability of the Proposed Model to Predict Electric Field Waveforms Measured at 14.7 km

Figures 5 and 6 present the electric field obtained by using the proposed model with the parameters given in Tables 3 and 4. The values of the parameters were selected by trial and error to obtain a good fit between the measured electric fields and the simulated waveforms. From the listed parameters, H, which is the height of the junction point, is common to the main channel and the branch. Excellent agreement can be observed in Figures 5a and 6a between the simulated and the measured electric fields. It can be observed in Figures 5b and 6b that the total field at late times is affected by the field from Branch A.

Note that the height of the tip of the Säntis Tower is about 2,600 m above sea level. The median height of the −10° isotherm (which is thought to be indicative of the main negative charge region (Krehbiel, 1986) is estimated to be about 4,000-m ASL (Azadifar et al., 2016; this is also consistent with the height of lightning

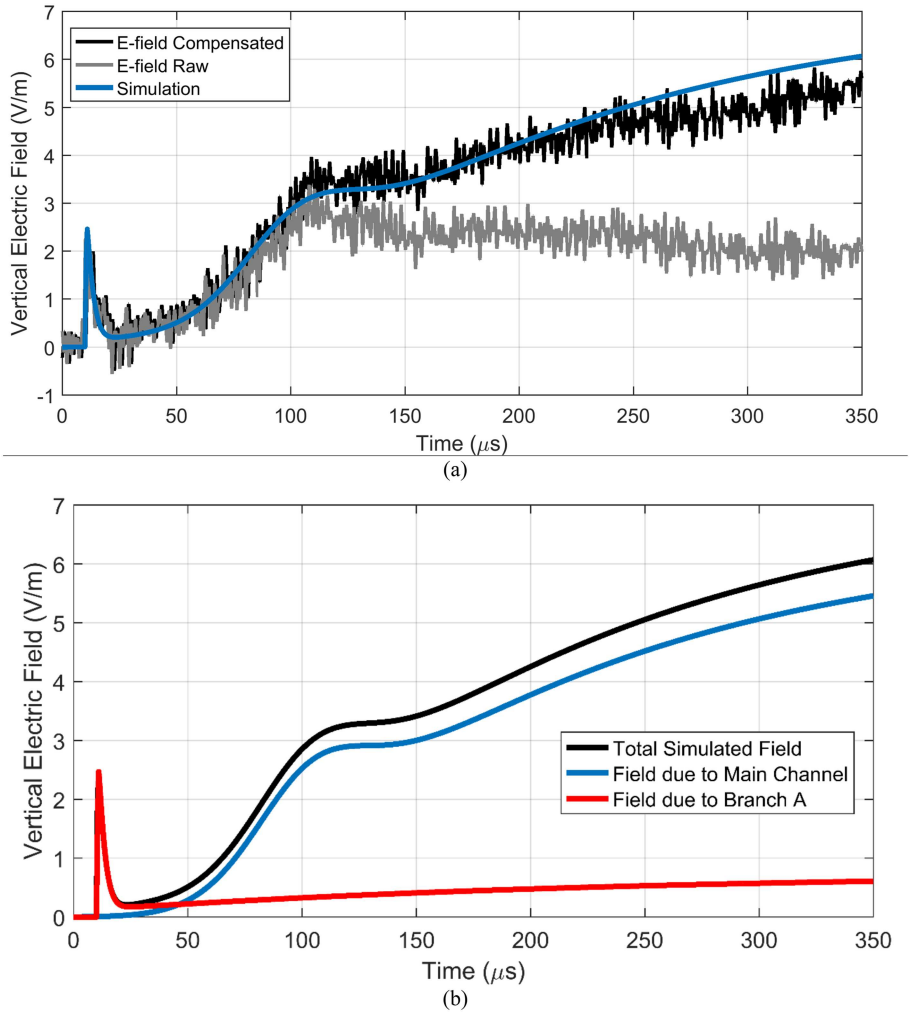

Figure 6. Vertical electric field computed using the model proposed in the paper. The lightning flash occurred on 21 October 2014, at 20:42:50. (a) Simulated vertical electric field versus measured field. (b) Contribution of main channel and of Branch A to the total electric field.

discharges found in the unpublished LMA lightning observations at the Säntis Tower. As a result, the estimated heights for the main channel above the tower tip of 1,100 and 1,400 m are reasonable for the particular case of Säntis Tower lightning events. Note that similar values are obtained in He, Azadifar, Rachidi, et al. (2018).

Table 3
Parameters providing the best fit of simulated and measured fields for Example 1 (see Figure 5)

Quasi-RS parameters		M-event parameters	
RS speed (V_0)	1.05×10^8 m/s	Wavefront speed (V_1)	0.7×10^8 m/s
Junction height (H)	1,100 m	Height of channel (H)	1,100 m
Attenuation constant (λ_0)	400 m	Reflection coefficient (R_g)	0.8
Length of branch (L_0)	8,000 m		
Inclination angle (θ_0)	73^o		
Azimuth angle (φ_0)	90^o		
Charge calibration factor*(q)	1.9		

*This factor was applied to conserve the charge at the junction point.

Table 4
Parameters providing the best fit of simulated and measured fields for Example 2 (see Figure 6)

Quasi-RS parameters		M-event parameters	
RS speed (V_0)	10^8 m/s	Wavefront speed (V_1)	0.8×10^8 m/s
Junction height (H)	1,400 m	Height of channel (H)	1,400 m
Attenuation constant (λ_0)	500 m	Reflection coefficient (Rg)	0.8
Length of branch (L_0)	8,000 m		
Inclination Angle (θ_0)	73^o		
Azimuth Angle (φ_0)	90^o		
Charge Calibration factor*(q)	3.4		

*This factor was applied to conserve the charge at the junction point.

Our analysis shows that the millisecond-scale pulse is primarily influenced by the height of the junction point (H) and the ground reflection coefficient (R_g). The speed of the M component wave, v_1, on the other hand, does not influence the waveform significantly.

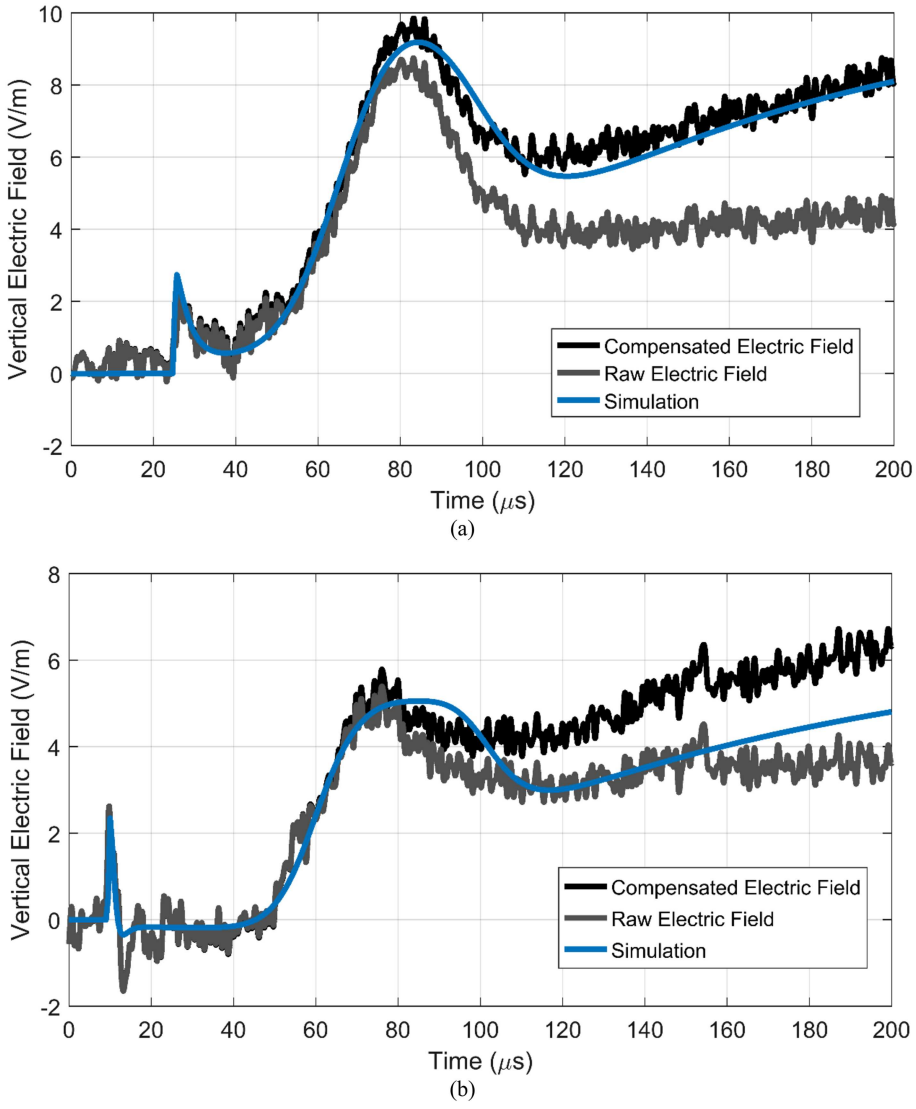

Figure 7. Vertical electric field computed using the model proposed in the paper. (a) The lightning flash occurred on 21 October 2014, at 20:42:50. (b) The lightning flash occurred on 22 October 2014, at 01:13:36.

Table 5
Parameters providing the best fit of simulated and measured fields for Example 3 (see Figure 7A)

Quasi-RS parameters		M-event parameters	
RS speed (V_0)	1×10^8 m/s	Wavefront speed (V_1)	0.9×10^8 m/s
Junction height (H)	1,500 m	Height of channel (H)	1,500 m
Attenuation constant (λ_0)	800 m	Reflection coefficient (Rg)	0.8
Length of branch (L_0)	8,000 m		
Inclination Angle (θ_0)	80^o		
Azimuth Angle (φ_0)	90^o		
Charge Calibration factor*(q)	4		

*This factor was applied to conserve the charge at the junction point.

The shape of the fast microsecond-scale pulse is essentially determined by the assumed current in the branch, the RS velocity v_0, the attenuation constant used in the MTLE model (λ_0), the inclination angle of the branch θ_0, and the azimuth angle of the branch φ_0. The length of Branch A (L_0) does not play a significant role.

To summarize, the proposed model is able to predict the observed electric field at 14.7 km for measured channel-base currents, including the fast, microsecond-scale pulse.

To further validate the model, two more cases were considered. Figures 7a and 7b show the simulation results in comparison with the electric field waveforms measured at 14.7 km. The parameters of the model for the cases presented in Figures 7a and 7b are given in Tables 5 and 6, respectively. A reasonable agreement between the simulation results and the measured waveforms is evident, although the undershoot of the electric field in Figure 7b could not be completely reproduced. Our analysis has shown that the obtained result can be improved by modifying the RS-like current wave in the branch by shortening the tail of the current waveform.

6.2. Ability of the Proposed Model to Reproduce Observed Electric Field Features at Various Ranges

In this section, we discuss the effect on the fields at various distances of the input parameters of our model. We show that selecting the values of the parameters within physically plausible ranges leads to successful reproduction of the observed electric field waveform features. These parameters are (1) observation point, (2) geometry of the branch, and (3) velocity of wave propagation along the branch.

6.2.1. Distance to the Lightning Channel and Branch Azimuth Angle

In order to investigate the effect of distance and branch azimuth angle (φ_0), we calculated the vertical electric field using the parameters (other than φ_0) given in Table 3. We simulated the fields at 1, 5, 15, and 100 km making the azimuth angle φ_0 (see Figure 4) equal to 0°, 30°, 60°, 90°, 120°, 150°, and 180°. Results are presented in Figure 8. The following can be seen from that figure:

1. At 1 km, the microsecond-scale pulses are negligible compared to the millisecond-scale pulses (Figure 8a).

Table 6
Parameters providing the best fit of simulated and measured fields for Example 3 (see Figure 7B)

Quasi-RS parameters		M-Event Parameters	
RS speed (V_0)	1.5×10^8 m/s	Wavefront speed (V_1)	0.9×10^8 m/s
Junction height (H)	1,900 m	Height of channel (H)	1,900 m
Attenuation constant (λ_0)	200 m	Reflection coefficient (Rg)	0.8
Length of branch (L_0)	8,000 m		
Inclination Angle (θ_0)	60^o		
Azimuth Angle (φ_0)	90^o		
Charge Calibration factor*(q)	4		

*This factor was applied to conserve the charge at the junction point.

Table 7
Chosen parameters to compute DRR values

Quasi-RS parameters		M-event parameters	
RS speed (V_0)	Swipe = 1×10^8 to 1.5×10^8 m/s	Wavefront speed (V_1)	Constant = 0.7×10^8 m/s
Junction height (H)	Swipe = 500 to 2,000 m	Height of channel (H)	Swipe = 500 to 2,000 m
Attenuation constant (λ_0)	Constant = 400 m	Reflection coefficient (R_g)	Constant = 0.8
Length of branch (L_0)	Constant = 8,000 m		
Inclination angle (θ_0)	Swipe = 50 to 120°		
Azimuth angle (φ_0)	Swipe = 0 to 90°		
Charge calibration factor*(C_q)	Constant = 1.9		

*This factor was applied to conserve the charge at the junction point.

2. At 15 and 100 km and φ_0 close to 90°, the microsecond-scale pulses become comparable and even dominant compared to the millisecond-scale pulses (Figures 8c and 8d).
3. At 15 and 100 km and φ_0 close to 0 or 180°, the microsecond-scale pulses become negligible compared to the millisecond-scale pulses (Figures 8c and 8d).

The proposed model predicts bipolar microsecond-scale pulses when the azimuth angle is either between −45° and 45° or between 135° and 225°. Our analysis also shows that longer tails of the RS-like currents in the branch will lead to more unipolar pulses and vice versa.

6.2.2. Branch Polar Angle

Here, we evaluate the effect of the branch polar angle (θ_0) on the calculated vertical electric field waveform. We simulated the field at 15-km distance, for θ_0 equal to 10°, 30°, 70°, 90°, 110°, and 130° and for φ_0 equal to 90°. It should be noted that the chance of having an angle θ_0 greater than 90° is low, especially in the case of upward flashes. All other parameters are the same as those in Table 3.

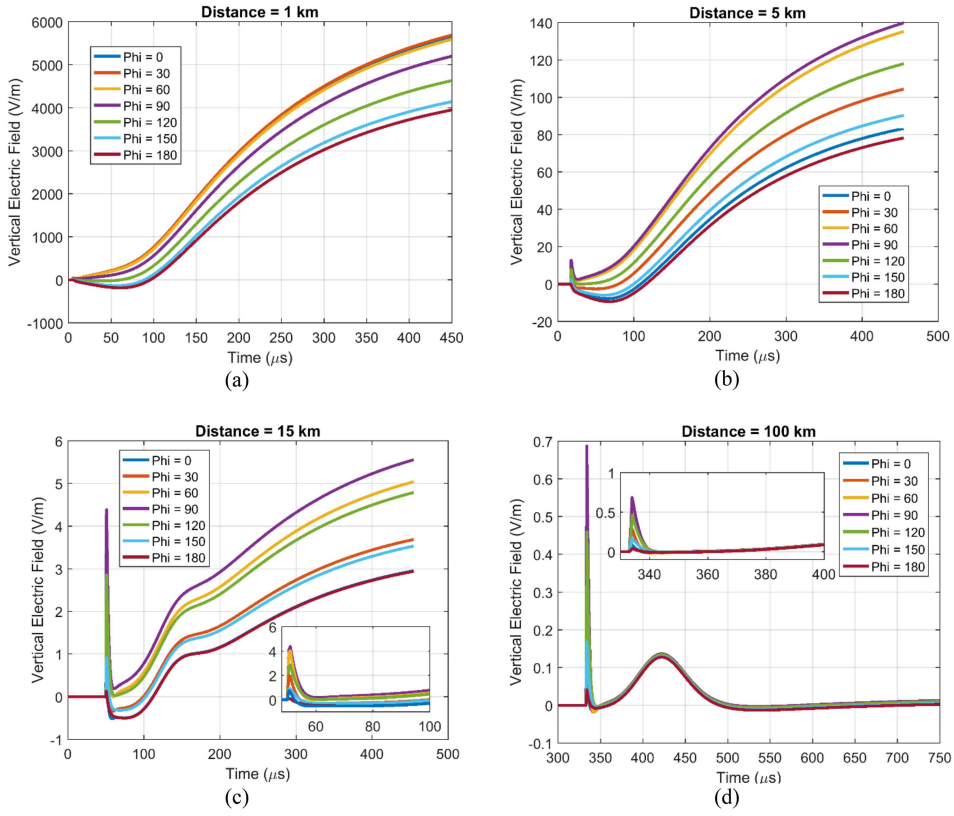

Figure 8. Simulated vertical electric field at 1, 5, 15, and 100 km at azimuth angles φ_0 equal to 0, 30°, 60°, 90°, 120°, 150°, and 180°. The other parameters of the model are the same as in Table 3.

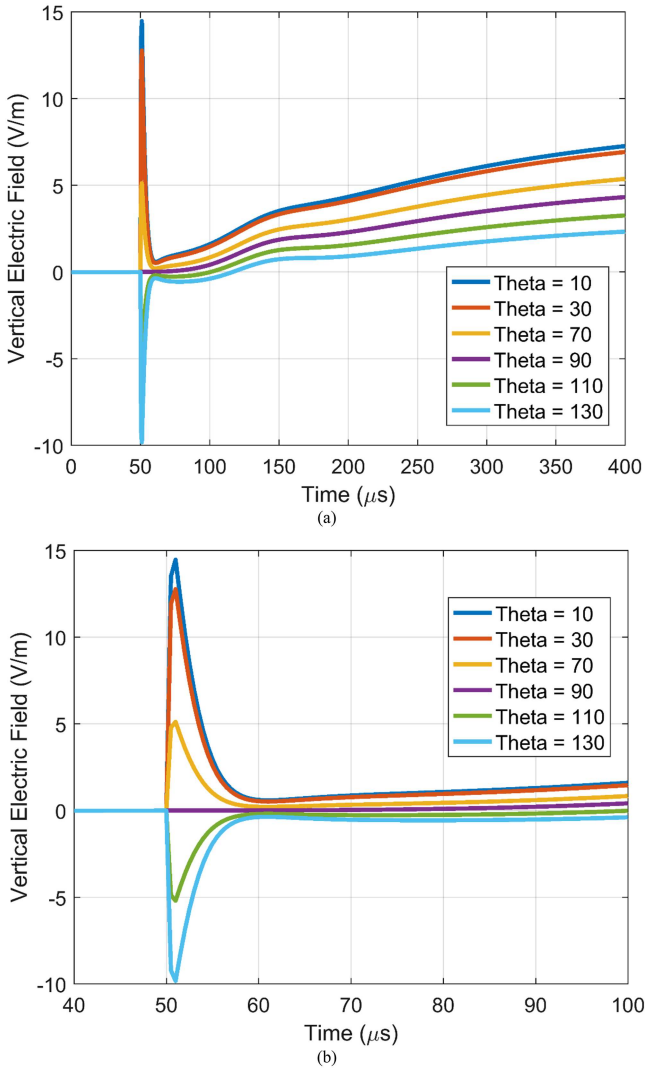

Figure 9. Simulated vertical electric field at 15 km at inclination (polar) angles θ_0 equal to 10°, 30°, 70°, 90°, 110°, and 130°. (a) Overall waveform. (b) Expanded view.

Figure 9 presents the obtained results. The following can be seen in the figure:

1. For θ_0 equal to 90°, the microsecond-scale pulse vanishes.
2. For θ_0 smaller than 90°, the microsecond-scale pulses have the same polarity as the millisecond-scale pulse.
3. For θ_0 greater than 90°, the microsecond-scale pulses have polarity opposite to that of the millisecond-scale pulse.

6.2.3. Velocity of the RS-Like Wave Propagating Along the Branch

Figure 10 shows the simulated vertical electric field at 15 km from the main lightning channel. The wave propagation velocity along Branch A is set to 1×10^8, 1.25×10^8, and 1.5×10^8 m/s. The (polar) inclination angle of the discharge, θ_0, is fixed at 50°, and the azimuth angle, φ_0, is equal to 0°. All other parameters are the same as those in Table 3. As the velocity of the RS-like wave, the larger the amplitude of the microsecond-scale pulse.

6.3. Classification of Distance Ranges From the M Component Field Perspective

We have shown in sections 6.1 and 6.2 that the obtained electric field waveforms are dependent on the model parameters and most importantly on the geometry of the branch. We suggest a possible method to define two distance ranges: Close range and middle-and-far distance ranges based on the model proposed in section 5.

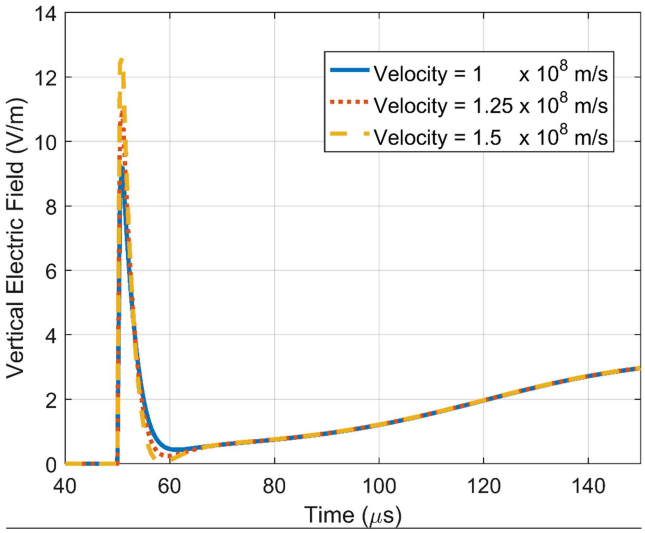

Figure 10. Simulated vertical electric field at 15 km. Propagation velocity along Branch A is set to 1×10^8, 1.25×10^8, and 1.5×10^8 m/s. The inclination angle of the discharge, θ_0, is fixed at 50°, and the azimuth angle, φ_0, is equal to 0°.

We define the Distance Range Ratio (DRR) as the ratio of the peak amplitudes of the microsecond-scale pulse at the start of the M component and of the ensuing millisecond-scale pulse:

$$\mathrm{DRR} = \frac{\text{Peak of Microsecond-scale Pulse}}{\text{Peak of Millisecond-scale Pulse}}. \tag{4}$$

We calculated the value of DRR using the parameters given in Table 3. We set the parameters that have only a minor effect on the peak of the microsecond- and the millisecond-scale pulses to constant values (V_1, R_g, L_0, λ_0, and, q), and we swept the other parameters (V_0, H, θ_0, and φ_0). We calculated the values of DRR for distances of 1, 2.5, 5, 7.5, 10, 15, and 20 km.

The obtained results show that at distances smaller than 5 km, the value of DRR is always smaller than 1. We use this result to define distances shorter than 5 km as close-range distances. At distances greater than 5 km, the DRR could take values either smaller or greater than 1, depending on the model parameters. We use that fact to define distances longer than 5 km as middle-and-far range distances.

The definition of the DRR parameter is intimately related to the model introduced in this paper. It should be noted that according to the definition of DRR given above, the close and the far ranges can be defined as follows:

Close range: Distances for which the value of DRR cannot be greater than 1, regardless of the choice of model parameters.

Far range: Distances for which the value of DRR can be greater than 1 for certain sets of model parameters.

Note that these definitions do not prohibit DRR from being equal to zero for certain sets of model parameters at the far range. Specifically, DRR is equal to 0 for $\theta_0 = 0$. This fact is consistent with the observed electric field waveforms of M components, in which, at far distances, the microsecond-scale pulses can be either present or absent.

7. Summary

We developed a new model of engineering type that can reproduce the observed electric field signatures of M component processes at both close and far distances, including the microsecond-scale connecting pulses. Two channels are involved in the model: (1) The main channel, which carries a steady current (ICC or CC following the RS) to ground, and (2) a floating, typically in-cloud channel, which can be a previously

created but decayed branch that gets reactivated by a recoil leader or a newly formed branch created by an independent leader, which we call Branch A.

The model assumes a guided-wave process (including the reflection from ground) in the main channel and a RS-like process in Branch A. The results of simulations show excellent agreement with the measured electric fields at 14.7-km distance from the tower. It should be noted that the parameters of the model were adjusted to achieve a good match with the experimental results. The proposed model can also reproduce the electric field signatures of M components at shorter and longer distances.

Acknowledgments
Financial supports from the Swiss National Science Foundation (Projects 200021_147058 and 200020_175594) and the European Union's Horizon 2020 Research and Innovation Programme (Grant 737033-LLR) are acknowledged. Participation of VAR was supported in part by NSF Grant AGS-1701484 and RSF Grant 19-17-00218. This study complies with the AGU data policy. All the data are available online at Zenodo repository (doi:10.5281/zenodo.3438337).

References

Azadifar, M., Lagasio, M., Fiori, E., Rachidi, F., Rubinstein, M., & Procopio, R. (2016). Occurrence of downward and upward flashes at the Säntis Tower: Relationship with-10 degrees C temperature altitude. In *European Electromagnetics International Symposium EUROEM*.

Azadifar, M., Paolone, M., Pavanello, D., Romero, C., Rachidi, F., & Rubinstein, M. (2014). An update on the instrumentation of the Säntis Tower in Switzerland for lightning current measurements and obtained results. In *CIGRE International Colloquium on Lightning and Power Systems. Lyon, France*.

Campos, L. Z. S., Saba, M. M. F., Pinto, O., & Ballarotti, M. G. (2007). Waveshapes of continuing currents and properties of M-components in natural negative cloud-to-ground lightning from high-speed video observations. *Atmospheric Research*, *84*, 302–310. https://doi.org/10.1016/J.ATMOSRES.2006.09.002

Fisher, R. J., Schnetzer, G. H., Thottappillil, R., Rakov, V. A., Uman, M. A., & Goldberg, J. D. (1993). Parameters of triggered-lightning flashes in Florida and Alabama. *Journal of Geophysical Research*, *98*, 22887. https://doi.org/10.1029/93JD02293

Flache, D., Rakov, V. A., Heidler, F., Zischank, W., & Thottappillil, R. (2008). Initial-stage pulses in upward lightning: Leader/return stroke versus M-component mode of charge transfer to ground. *Geophysical Research Letters*, *35*, 2–6. https://doi.org/10.1029/2008GL034148

He, L., Azadifar, M., Li, Q., Rubinstein, M., Rakov, V. A., Mediano, A., et al. (2018). Modeling of different charge transfer modes in upward flashes constrained by simultaneously measured currents and fields. In *Joint IEEE EMC and Asia Pacific EMC Symposium. Singapore*.

He, L., Azadifar, M., Rachidi, F., Rubinstein, M., Rakov, V. A., Cooray, V., et al. (2018). An analysis of current and electric field pulses associated with upward negative lightning flashes initiated from the Säntis Tower. *Journal of Geophysical Research – Atmospheres*, *123*, 4045–4059. https://doi.org/10.1029/2018JD028295

Jiang, R., Qie, X., Yang, J., Wang, C., & Zhao, Y. (2013). Characteristics of M-component in rocket-triggered lightning and a discussion on its mechanism. *Radio Science*, *48*, 597–606. https://doi.org/10.1002/rds.20065

Jiang, R.-B., Sun, Z.-L., & Wu, Z.-J. (2014). Concurrent upward lightning flashes from two towers. *Atmospheric and Oceanic Science Letters*, *7*, 260–264. https://doi.org/10.1080/16742834.2014.11447171

Jordan, D. M., Idone, V. P., Orville, R. E., Rakov, V. A., & Uman, M. A. (1995). Luminosity characteristics of lightning M components. *Journal of Geophysical Research*, *100*(D12), 25695. https://doi.org/10.1029/95jd01362

Krehbiel, P. R. (1986). *The electrical structure of thunderstorms, in: The Earth's electrical environment*, (pp. 90–113). Washington, D. C: National Academy Press.

Malan, D. J., & Collens, H. (1937). Progressive lightning: III. The fine structure of return lightning strokes. *Proceedings of the Royal Society of London. Series A - Mathematical and Physical Sciences*, *162*, 175–203. https://doi.org/10.1098/rspa.1937.0175

Malan, D. J., & Schonland, B. F. J. (1947). Progressive lightning; directly-correlated photographic and electrical studies of lightning from near thunderstorms. *Proceedings of the Royal Society of London. Series A: Mathematical and Physical Sciences*, *191*, 485–503. https://doi.org/10.1098/RSPA.1947.0129

Mazur, V., & Ruhnke, L. H. (2011). Physical processes during development of upward leaders from tall structures. *Journal of Electrostatics*, *69*, 97–110. https://doi.org/10.1016/j.elstat.2011.01.003

Miki, M., Rakov, V. A., Shindo, T., Diendorfer, G., Mair, M., Heidler, F., et al. (2005). Initial stage in lightning initiated from tall objects and in rocket-triggered lightning. *Journal of Geophysical Research*, *110*, D02109. https://doi.org/10.1029/2003JD004474

Montanyà, J., van der Velde, O., & Williams, E. R. (2015). The start of lightning: Evidence of bidirectional lightning initiation. *Scientific Reports*, *5*, 15180. https://doi.org/10.1038/srep15180

Nucci, C. A., Mazzetti, C., Rachidi, F.,Ianoz, M. (1988). On lightning return stroke models for LEMP calculations. In: 19th International Conference on Lightning Protection.

Paul, C., & Heidler, F. H. (2018). Properties of three types of M-components and ICC-pulses from currents of negative upward lightning measured at the Peissenberg Tower. *IEEE Transactions on Electromagnetic Compatibility*, 1–8. https://doi.org/10.1109/TEMC.2018.2802720

Qie, X., Jiang, R., Wang, C., Yang, J., Wang, J., & Liu, D. (2011). Simultaneously measured current, luminosity, and electric field pulses in a rocket-triggered lightning flash. *Journal of Geophysical Research*, *116*, D10102. https://doi.org/10.1029/2010JD015331

Rachidi, F., &Nucci, C. (1990). On the Master, Uman, Lin, Standler and the modified transmission line lightning return stroke current models. *Journal of Geophysical Research: Atmospheres*, *95*(D12), 20,389–20,393.

Rachidi, F., Janischewskyj, W., Hussein, A. M., Nucci, C. A., Guerrieri, S., Kordi, B., & Chang, J.-S. (2001). Current and electromagnetic field associated with lightning-return strokes to tall towers. *IEEE Transactions on Electromagnetic Compatibility*, *43*, 356–367. https://doi.org/10.1109/15.942607

Rakov, V. A., Crawford, D. E., Rambo, K. J., Schnetzer, G. H., Uman, M. A., & Thottappillil, R. (2001). M-compoenent mode of charge transfer to ground in lightning discharge. *Journal of Geophysical Research – Atmospheres*, *106*, 22817–22831. https://doi.org/10.1029/2000jd000243

Rakov, V. A., Thottappillil, R., & Uman, M. A. (1992). Electric field pulses in K and M changes of lightning ground flashes. *Journal of Geophysical Research – Atmospheres*, *97*, 9935–9950. https://doi.org/10.1029/92JD00797

Rakov, V. A., Thottappillil, R., Uman, M. A., & Barker, P. P. (1995). Mechanism of the lightning M component. *Journal of Geophysical Research*, *100*, 25701. https://doi.org/10.1029/95JD01924

Rakov, V. A., Uman, M. A., Hoffman, G. R., Masters, M. W., & Brook, M. (1996). Bursts of pulses in lightning magnetic radiation: Observations and locations for lightning test standards. *IEEE Transactions on Electromagnetic Compatibility*, *38*. https://doi.org/10.1109/15.494618

Romero, C., Paolone, M., Rubinstein, M., Rachidi, F., Rubinstein, A., Diendorfer, G., et al. (2012). A system for the measurements of lightning currents at the Säntis Tower. *Electric Power Systems Research*, *82*, 34–43. https://doi.org/10.1016/j.epsr.2011.08.011

Rubinstein, M., Bermdez, J., Rakov, V., Rachidi, F., & Hussein, A. (2012). Compensation of the instrumental decay in measured lightning electric field waveforms. *IEEE Transactions on Electromagnetic Compatibility*, *54*, 685–688. https://doi.org/10.1109/TEMC.2012.2198482

Shao, X. M., Krehbiel, P. R., Thomas, R. J., & Rison, W. (1995). Radio interferometric observations of cloud-to-ground lightning phenomena in Florida. *Journal of Geophysical Research*, *100*, 2749. https://doi.org/10.1029/94JD01943

Stolzenburg, M., Marshall, T. C., Karunarathne, S., Karunarathna, N., & Orville, R. E. (2015). An M-component with a concurrent dart leader traveling along different paths during a lightning flash. *Journal of Geophysical Research – Atmospheres*, *120*, 10,267–10,284. https://doi.org/10.1002/2015JD023417

Thottappillil, R., Goldberg, J. D., Rakov, V. A., Uman, M. A., Fisher, R. J., & Schnetzer, G. H. (1995). Properties of M components from currents measured at triggered lightning channel base. *Journal of Geophysical Research*, *100*, 25711. https://doi.org/10.1029/95JD02734

Tran, M. D., & Rakov, V. A. (2019). An advanced model of lightning M-component. *Journal of Geophysical Research – Atmospheres*, *124*, 2296–2317. https://doi.org/10.1029/2018JD029604

Tran, M.D., Rakov, V.A., Ngin, T., Gamerota, W.R., Pilkey, J.T., Uman, M.A., Jordan, D.M., 2013. Microsecond-scale electric field pulses associated with lightning M-components. Am. Geophys. Union, Fall Meet. 2013, Abstr. #AE13B-0356.

Visacro, S., Araujo, L., Guimarães, M., & Vale, M. H. M. (2013). M-component currents of first return strokes in natural negative cloud-to-ground lightning. *Journal of Geophysical Research – Atmospheres*, *118*, 12,132–12,138. https://doi.org/10.1002/2013JD020026

Wang, J., Quanxin, L., Tao, Z., Qinghua, Z., Li, C., Yadong, F., & Gen, Q. (2017). Far electric field waveform in triggered lightning. In *Asia-Pasific International Conference on Lightning. Thailand*.

Warner, T. A., Saba, M. M. F., Schumann, C., Helsdon, J. H., & Orville, R. E. (2016). Observations of bidirectional lightning leader initiation and development near positive leader channels. *Journal of Geophysical Research – Atmospheres*, *121*, 9251–9260. https://doi.org/10.1002/2016JD025365

Winn, W. P., Eastvedt, E. M., Trueblood, J. J., Eack, K. B., Edens, H. E., Aulich, G. D., et al. (2012). Luminous pulses during triggered lightning. *Journal of Geophysical Research – Atmospheres*, *117*. https://doi.org/10.1029/2011JD017105

Yoshida, S., Biagi, C. J., Rakov, V. A., Hill, J. D., Stapleton, M. V., Jordan, D. M., et al. (2012). The initial stage processes of rocket-and-wire triggered lightning as observed by VHF interferometry. *Journal of Geophysical Research – Atmospheres*, *117*. https://doi.org/10.1029/2012JD017657

Zhang, Q., Yang, J., Liu, M., & Wang, Z. (2011). Measurements and simulation of the M-component current and simultaneous electromagnetic fields at 60 m and 550 m. *Atmospheric Research*, *99*, 537–545. https://doi.org/10.1016/J.ATMOSRES.2010.12.011

Zhang, Y., Zhang, Y., Xie, M., Zheng, D., Lu, W., Chen, S., & Yan, X. (2016). Characteristics and correlation of return stroke, M component and continuing current for triggered lightning. *Electric Power Systems Research*, *139*, 10–15. https://doi.org/10.1016/J.EPSR.2015.11.024

Zhou, H., Rakov, V. A., Diendorfer, G., Thottappillil, R., Pichler, H., & Mair, M. (2015). A study of different modes of charge transfer to ground in upward lightning. *Journal of Atmospheric and Solar - Terrestrial Physics*, *125–126*, 38–49. https://doi.org/10.1016/j.jastp.2015.02.008

Zhou, M., Wang, D., Wang, J., Takagi, N., Gamerota, W. R., Uman, M. A., et al. (2014). Correlation between the channel-bottom light intensity and channel-base current of a rocket-triggered lightning flash. *Journal of Geophysical Research – Atmospheres*, *119*, 13,457–13,473. https://doi.org/10.1002/2014JD022367